# Free Form Fabrication Using the Laser Engineered Net Shaping (LENS™) Process

D. M. Keicher, J. A. Romero, C. L. Atwood, J. E. Smugeresky*,
M. L. Griffith, F. P. Jeantette, L. D. Harwell and D. L. Greene

Sandia National Laboratories
Albuquerque, New Mexico 87185-1411
*Livermore, California 94551-0969



## ABSTRACT

Sandia National Laboratories is developing a technology called Laser Engineered Net Shaping™ (LENS™). This process allows complex 3-dimensional solid metallic objects to be directly fabricated from a CAD solid model. Experiments performed demonstrate that complex alloys such as Inconel™ 625 and ANSI stainless steel alloy 316 can be used in the LENS™ process to produce solid metallic shapes. In fact, the fabricated structures exhibit grain growth across the deposition layer boundaries. Mechanical testing data of deposited 316 stainless steel material indicates that the deposited material strength and elongation are greater than that reported for annealed 316 stainless steel. Electron microprobe analysis of the deposited Inconel™ 625 material shows no compositional degradation of the 625 alloy and that 100% dense structures can be obtained using this technique. High speed imaging used to acquire process data during experimentation shows that the powder particle size range can significantly affect the stability, and subsequently, the performance of the powder deposition process. Finally, dimensional studies suggest that dimensional accuracy to ±0.002" ( in the horizontal direction) can be maintained.



## INTRODUCTION

Lasers have gained wide spread acceptance over the last two decades as a useful tool for industrial materials processing applications. Laser cladding of similar and/or dissimilar materials for improved wear properties, corrosion resistance, thermal barrier coatings, etc. has been investigated extensively[1-4]. Models have been developed to describe some of the physical phenomenon which occur during the laser cladding process[5,6]. Other studies have been performed to investigate process interactions, such as the laser absorption by the metal powder[7], and to measure the surface temperature of the cladding layer during processing[8]. More recently, the explosive growth in the area of rapid prototyping has prompted several groups to investigate the feasibility of using a process similar to the laser cladding process for producing solid metal objects[9,10]. As far back as 1984, the concept of using laser powder or wire deposition to rebuild and/or produce solid geometries has existed[11].

## DISCLAIMER

Sandia National Laboratories is developing a process called Laser Engineered Net Shaping™ (LENS™). This process allows complex 3-dimensional solid metallic objects to be directly fabricated from a CAD solid model. Currently, this process functions similar to a stereo lithography process. A faceted file is generated from the CAD solid model and then sliced into a sequence of layers. The sliced file is then input into another interpreter program which converts the sliced file into a series of tool path patterns required to build the entire layer. The component is fabricated by first generating an outline of the key component features and then filled using a rastering technique. This file is then used to drive the laser system to produce the desired component one layer at a time. This process differs from state of the art rapid prototyping (RP) processes in that a fully dense, metallic component can be produced using this system.

The current approach used to mature this technology focuses on first developing a fundamental understanding of the process. Experiments have been performed to identify the process parameters which affect the LENS™ process variability. The results of these experiments have been used to develop response surface models for process optimization[12] and then to identify process control methodologies. The results of these experiments are reported below.

## EXPERIMENT

Two laser systems have been used to develop the LENS™ process. The research platform consists of: an 1.8 kW cw Nd:YAG laser, a controlled atmosphere glovebox, a 4-axis computer controlled positioning system and a powder feed unit. The applications platform consists of: a 500W cw Nd:YAG laser, a controlled atmosphere glovebox, a 3-axis computer controlled positioning system and a powder feed unit. The positioning stages were mounted inside a controlled atmosphere glove box operating at a nominal oxygen level of 2-3 parts per million. The glove box atmosphere was Ar. The beam is brought into the glovebox through a window mounted on the top of the glovebox and directed to the deposition region using a six inch focal length plano-convex lens. The powder delivery nozzle is designed to inject the powder stream directly into the focused laser beam. The lens and powder nozzle move as an integral unit.

A schematic representation of the LENS™ process is shown in Fig. 1. The laser beam is focused onto a solid substrate, used as base for building an object, to create a molten puddle. The substrate is generally the same material as the powder being deposited. Powder particles are simultaneously injected into the puddle to build-up each layer. The substrate is moved beneath the laser beam to deposit a thin metal line to create the desired geometry for each layer. After deposition of each layer, the powder delivery nozzle and focus lens assembly is incremented away from the substrate a distance equal to the layer thickness to maintain a constant focus position. The powder is delivered to the deposition region via a carrier gas and the powder volume is regulated by a powder feed unit.

Experiments were performed on a variety of materials of which most were metals. Statistically designed experiments were done using Inconel™ 625 to identify significant process variables and to begin to understand the deposition process. A list of the process variables considered for these experiments are given in Table 1. The response variables used in evaluating the experimental results were: the material build-up height, the melt depth into the previous layer and the ratio of these two variables. The tests were performed by depositing ten layers of metal in a single wall for each of the experimental conditions. The material was deposited in only one direction of travel. Diagnostics used during this experimentation included: laser Doppler velocimetry, time resolved

infrared imaging, high magnification, high speed digital imaging and standard video imaging. Metallography and electron microprobe analysis were performed to measure the response variables and to evaluate the experiment results. These results were then used to develop relationships for deposition interactions. Two powder mesh sizes were used for the alloy 625 experiments. All of the build-up experiments were performed using a -80 to +325 mesh while a -325 mesh size powder was included in the high speed imaging tests to observe the effect of powder particle size on the deposition process in the powder/beam interaction zone.

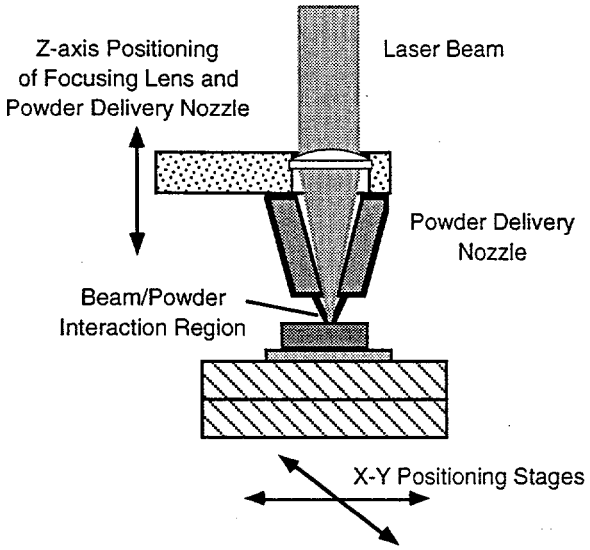


**Figure 1.** Configuration used in performing powder deposition experiments.

| Input Variable | Low | Medium | High |
|---|---|---|---|
| Laser Irradiance ($W/mm^2$) | 345 | 549 | 774 |
| Travel Sped (mm/s) | 8.47 | 21.17 | 33.87 |
| Z-Axis Increment | 0.127 | 0.229 | 0.381 |
| Powder Volume (gm/min.) | 1.785 | 2.418 | 3.057 |
| Carrier Gas Pressure (MPa) | 0.14 | - | 0.21 |
| Powder Velocity (mm/s) | 5000 | - | 6500 |

**Table 1.** Process variables considered for statistically designed experiments.

Subsequent experiments were performed using ANSI stainless steel alloy 316 powder (nominal composition) to develop the LENS™ process for fabricating complex three-dimensional components directly from the CAD solid model. CAD solid models of an object were converted to an STL file and then sliced using several different slicing routines. After the slice file was created, an interpreter file was used to generate tool path information to drive the LENS™ system. The current approach focuses on identifying the limitations imposed on this process by current state-of-the-art fabrication techniques and then using the knowledge gained to improve the process. Thus

far, this work has focused on identifying angular limitations of the build, surface finish and dimensional accuracy of the solid part. Solid bars were fabricated from the 316 stainless steel material to mechanically evaluate the deposited structure. These specimens are also being used to determine the deposited stainless steel material properties (i.e. grain size, .

A Kodak Ektapro intensified and gated high speed digital imaging system was used to slow down the deposition process and allow observation of the beam/powder interaction in the deposition region. A schematic representation of the experimental arrangement is given in Fig. 3. To view through the intense laser plume, a 150 mW, 690 nm wavelength diode laser was used as an illumination source. A laser line filter was placed in the lens to filter out the broad band emission from the plume. For the high speed photography, two different powder sizes were used to observe the effect of powder size on the performance of the process. The powder size distributions for the two powders were: 50-180 μm for the larger powder size and <50 μm for the smaller powder size. The framing rate on the camera was 2000 pictures per second. A gate width of 50 μs was used at magnification of approximately 50x. The high speed photography results were also used to identify whether significant heating of the powder particles occurred prior to impingement into the deposition melt zone.

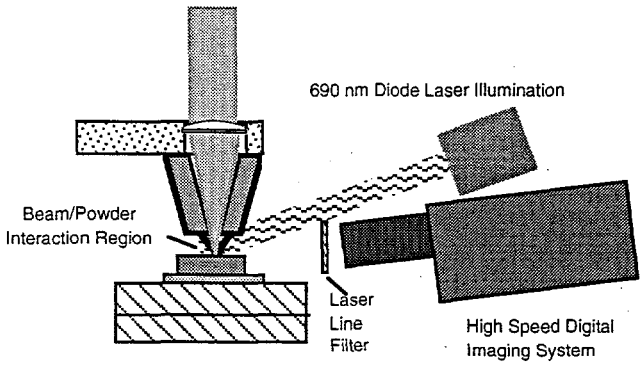


**Figure 3.** Schematic representation of arrangement used in high speed imaging of powder deposition process.

## RESULTS AND DISCUSSION

For the experiments using the Inconel™ 625 material, complete melting of the powder occurred for all the tests. In addition, textured grain growth of the deposited material occurred across the deposition layer boundary in nearly all cases. As mentioned previously, the two response variables considered for these tests were the material build-up height and the melt depth into the substrate. After the experiments were performed, metallographic cross-sections of all of the test samples were made. The response variables were measured from photographs taken of these metallographic cross-sections. The build-up height was measured from the original surface to the top of the deposited structure. Similarly, the melt depth was taken to be the depth of the dissolution region. A typical structure is shown in Fig. 4 (a) for the deposition occurring at 345 W/mm$^2$, 8.47 mm/s travel speed, a powder volume of 1.9 gm/min., a gas pressure of 0.14 MPa and a z-axis increment of 0.381 mm/pass. Figure 4 (b) shows the melt zone/substrate interface for the highest energy input parameters used in these experiments (774 W/mm$^2$, 1.9 gm/min. powder, 0.14 MPa carrier gas, 8.47 mm/s, z-increment 0.254 mm/pass). As can be seen from Fig. 4 (b), there was very little intergranular melting in the substrate region. The intergranular melting which has occurred (indicated by arrow), goes into the substrate only a fraction of the substrate grain size. This suggests, that for the conditions used in this testing, the heat affected zone is relatively small.

Figure 5 shows the melt depth into the substrate plotted as a function of the build-up height. For the experimental conditions used in these test, the melt depth varied from a minimum depth of 0.048 mm to a maximum depth of 0.273 mm. The build-up height varied from a minimum of 0.071 mm to a maximum of 1.730 mm. The data sets are identified by the laser power and travel speed associated with each condition. As shown in Fig. 5, the melt depth tends to increase with increasing laser power. As expected, the minimum melt depth occurs for the lowest laser power conditions, while the maximum melt depth tends to occur for the higher laser power conditions. There is, however, a great deal of overlap in the melt depth conditions for the intermediate and high power parameters. At all of the power levels, there is a significant increase in build-up of the deposited material as the component travel speed is decreased, with only a modest increase in the melt depth at that power. In general, the trend from this cursory analysis suggests that the penetration into the substrate occurs early in the deposition process. If the part is scanned under the beam at a slow rate of speed, then the powder is given time to build and slightly more penetration occurs due to the slow travel speed. Conversely, if the substrate is scanned under the beam at a high rate of speed, the penetration into the substrate is effected little and the build-up is inhibited. Indeed this is the case for all of the data in Fig. 5 at a build-up height of greater than 1 mm, deposited with a slow scan speed. In any case, it is apparent that the minimum penetration into the substrate occurs when the irradiance is low, yet sufficient to incur complete melting.

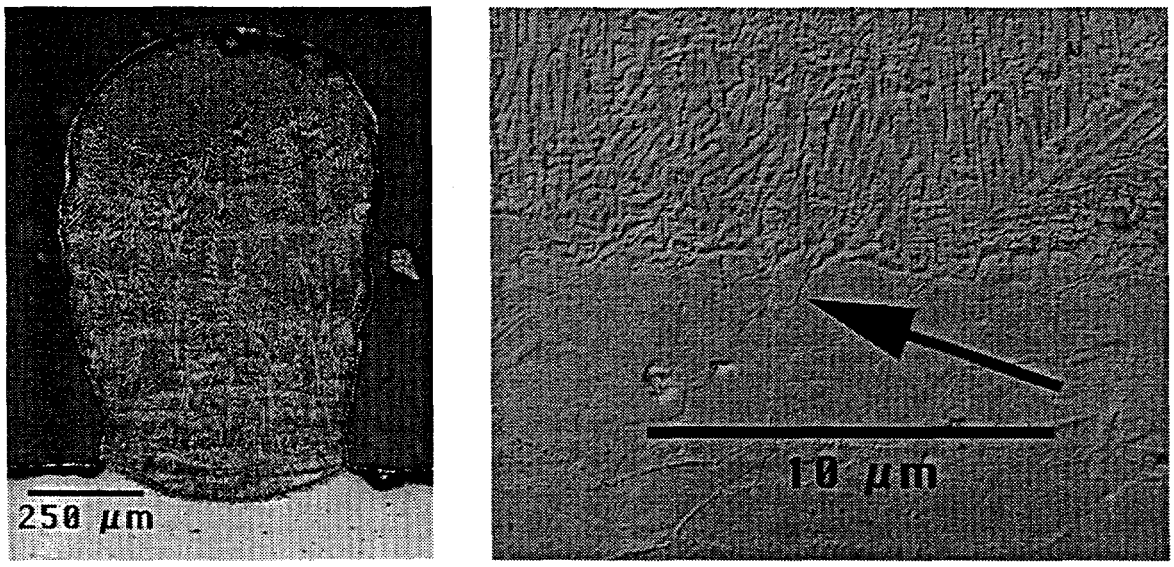


(a) (b)

**Figure 4.** Photomicrographs showing a) textured grain growth for laser deposited materials: 345 W/mm$^2$, 8.47 mm/s travel speed, a powder volume of 1.9 gm/min., a gas pressure of 0.14 MPa and a z-axis increment of 0.381 mm/pass, b) Melt zone/substrate region: 774 W/mm$^2$, 1.9 gm/min. powder, 0.14 MPa carrier gas, 8.47 mm/s, z-increment 0.254 mm/pass.

Although visual analysis of the sample cross-sections exhibited no obvious signs of porosity, electron microprobe analysis was performed using wavelength dispersive spectroscopy on selected samples at the test matrix extremum points to quantify this observation. Electron microprobe analysis provided a full quantitative analysis of the material density in both the substrate and deposited material and compared these measurements to those from a known standard. The results suggested that the density of the deposited material was slightly more dense than the substrate. They also indicated that there was no apparent difference in composition between the deposited material and the original substrate. These results were very encouraging.

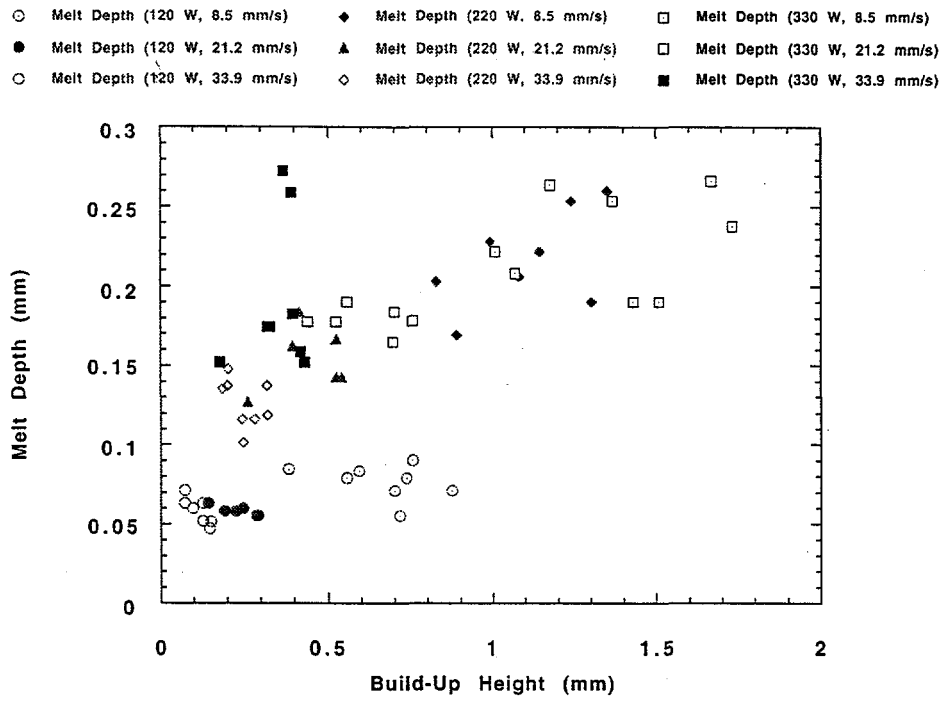


**Figure 5.** Measured results for melt depth and build-up height from experiment test matrix.

The data sets generated were analyzed using Minitab®, a statistical data analysis package, to develop response surface models for the LENS™ process. The software allows the user to identify statistically significant factors for process optimization. In depth results from this study are reported elsewhere[12]; however, what these experiments showed was that, for the factor space considered, laser irradiance and component velocity both played a significant role in the build-up and remelt processes. From these experimental results (see Fig. 5), it is obvious that reducing the laser irradiance subsequently reduces the melt depth into the substrate. However, this also reduces the build-up rate. Further analysis of these experimental results suggests that there was strong correlation of the material build-up height to the total volumetric exposure (laser irradiance/component velocity). In fact, increases were nearly linear with increasing exposure (see Fig. 6).

High speed, high magnification imaging allowed the LENS™ process to be effectively slowed down to visualize the molten metal/powder interaction region. The laser illumination eliminated the broadband emission associated with the laser generated plume and actually permitted the molten region to be observed for a qualitative analysis. For both particle sizes, it appears that particles do not become molten until they are, in fact, actually injected into the melted metal puddle in the deposition region. For the smaller particle size distribution, the melt puddle appeared to be stable and well behaved. For the larger particle size, however, the molten puddle was very energetic and unstable. For the larger powder size distribution, the particle size was a significant fraction of the deposition region width. Directing the larger particles into the molten deposition region caused a larger displacement of the liquid metal thus adding more energy to the oscillations of the melt pool. Further studies are required to draw more quantitative conclusions for the effects of particle size on the powder deposition process.

---

® MINITAB is a registered trademark of Minitab Inc.

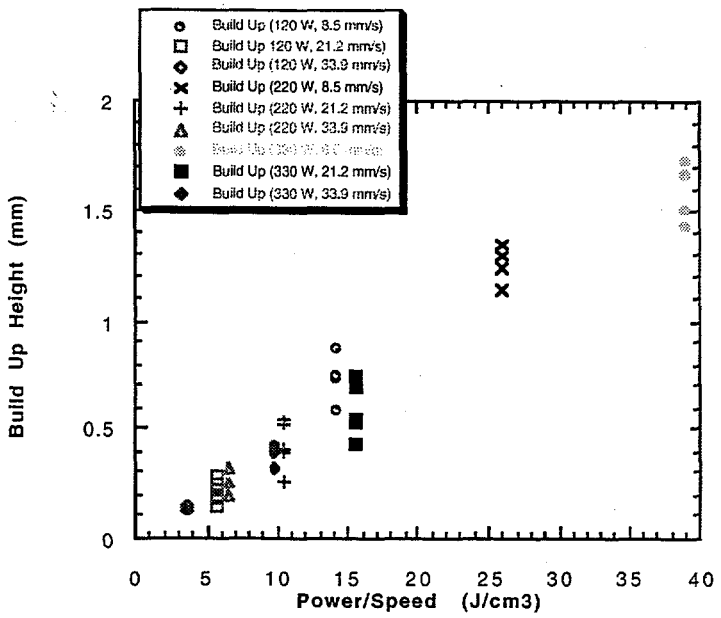


**Figure 6.** Plot of material build-up height vs. volumetric exposure for statistical designed experiment using Inconel™ 625 alloy.

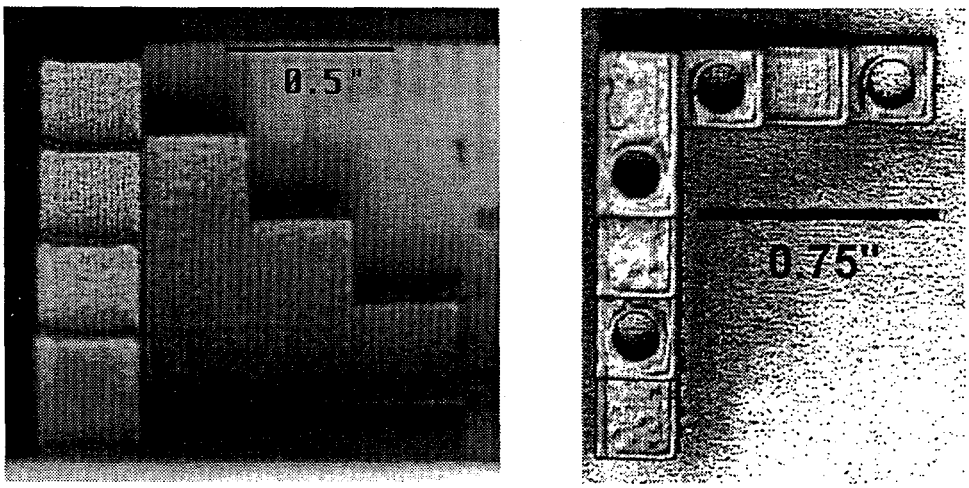


(a) (b)

**Figure 7.** Geometry used in accuracy studies (a) side view (b) top view.

Photographs of the geometry used to measure the dimensional accuracy of the LENS™ process are shown in Fig. 7. In building these components , it was determined that the dimensions in the plane normal to the beam optical axis could be maintained to less than ± 0.02 mm. The dimension in the growth direction (the direction parallel to the laser beam), however, could only be maintained within ± 0.4 mm. These results are extremely promising and further work will allow improvements in the dimensional accuracy to be achieved. Currently this process is being developed as a free-form fabrication process in which no support structures have been needed. Preliminary results from angle build studies suggest that the maximum angle which can be achieved in a single width deposition is approximately 30° draft. The surface finish appears to be

strong function of the powder particle size with the smaller powder particles giving a better surface finish. Although the surface finish of the "as built" component is somewhat rough, a small amount of finishing will produce an accurate, high polished surface.

Results from preliminary tensile testing of the deposited 316 stainless steel is given in Table 2. These bars were fabricated at 185 W, 50.8 cm/minute and 0.254 mm layer thickness. Two bars have been tested to date, each of which were built with different orientations: the first sample was built with its long axis normal to the beam optical axis and the second bar was fabricated with its long axis parallel to the beam optical axis. A third set of data is given for an annealed 316 stainless steel specimen[13]. In both cases, the yield strength of the fabricated 316 stainless steel bars significantly exceeds that for the reported value of the annealed baseline. For the horizontally fabricated bar, the yield strength is almost 2.5 times that for the annealed bar and the vertically fabricated bar is still almost a factor of two times that for the annealed bar. The elongation for the horizontally fabricated bar is less than that of the annealed material, while the vertically fabricated bar has an identical elongation of 50% (in 2.54 cm). Metallographic cross-sections of the horizontally fabricated structure showed that this structure exhibited no textured grain growth across the deposition layers. In fact, when the horizontally fabricated test specimen failed, there were some indications of delamination. The vertically fabricated bar did not exhibit the same delamination characteristics upon failure. Cross-sectional analysis of the vertical structure remains to be completed.

**Table 2.** Measured material tensile strength for LENS fabricated 316 stainless steel structures.

| Sample Orientation | Ultimate Tensile Strength (ksi) | Yield Strength (ksi) | Elongation (% in 2.54 cm) |
|---|---|---|---|
| Horizontal | 115 | 85 | 30 |
| Vertical | 115 | 60 | 50 |
| Annealed Bar | 85 | 35 | 50 |

## CONCLUSIONS

The feasibility of fabricating fully dense, solid metallic components directly from a CAD solid model was demonstrated. The material properties obtained, using alloys such as the Inconel™ 625 and ANSI stainless steel alloy 316, were comparable to wrought or cast materials and, in some cases, the material properties obtained in the LENS™ fabricated structure far exceed those for annealed metal stock. Dimensional studies demonstrated that very precise tolerances can be achieved in a horizontal build plane. The data generated from these studies has suggested ways to control and improve dimensional accuracy in the vertical fabrication direction. Further work is required to improve the material surface finish. Modified fabrication techniques need to be developed to overcome angular limitations imposed by the current fabrication approach.

## ACKNOWLEDGMENTS

We would like to thank Paul Hlava for his assistance in performing microprobe analyses. We would also like to thank Mike Hosking for his insightful input and technical review of this paper.

## REFERENCES


1) A. Frenk and J. D. Wagniere, "Laser Cladding with Cobalt-Based Hardfacing Alloys," J. Phys. IV, **1** (1991) p c7-65.

2) R. Subramanian, S. Sircar and J. Mazumder, "Laser Cladding of Zirconium on Magnesium for Improved Corrosion Properties," J. Mater. Sci. **26** (1991) p 951.

3) K. M. Jasim, R. D. Rawlings and D. R. F. West, "Thermal Barrier Coatings Produced by Laser Cladding," J. Mater. Sci. **25** (1990) p 4943.

4) J. De Damborenea and A. J. Vazquez, "Laser Cladding of High-Temperature Coatings," J. Mater. Sci. **28** (1993 p 4775.

5) S. Sircar, K. Chattopadhyay and J. Mazumder, "Nonequalibrium Synthesis of $NbAl_3$ and Nb-Al-V Alloys by Laser Cladding: Part I. Microstructure Evolution," Metall. Trans. A **23A** (1992) p 2419.

6) J. Mazumder and A. Kar, "Solid Solubility in Laser Cladding," J. Met. (Feb. 1987) p 18.

7) Y. Kizaki, H. Azuma, S. Yamazaki, H. Sugimoto and S. Takagi, "Phenomenological Studies in Laser Cladding. Part I. Time-Resolved Measurements of the Absorptivity of Metal Powder," Jpn. J. Appl. Phys. **32** (1993) p 205.

8) Y. Kizaki, H. Azuma, S. Yamazaki, H. Sugimoto and S. Takagi, "Phenomenological Studies in Laser Cladding. Part II. Thermometrical Experiments on the Melt Pool," Jpn. J. Appl. Phys. **32** (1993) p 213.

9) J. L. Koch and J. Mazumder, "Rapid Prototyping by Laser Cladding," ICALEO '93 Proc. **77** (1993) p 213.

10) D. M. Keicher, J. A. Romero, C. L. Atwood, J. G. Smugeresky, M. L. Griffith, F. P. Jeantette L. Harwell and D. Greene, "Laser Engineered Net Shaping (LENS™) for Additive Component Processing," Rapid Prototyping and Manufacturing '96 Proc., April, 1996.

11) U.S. Patent #4,323,756, "Method for Fabricating Articles by Sequential Layer Deposition," ( To Pratt and Whitney).

12) D. M. Keicher, J. L. Jellison, L. P. Schanwald, J. A. Romero and D. H. Abbott, "Towards a Reliable Laser Powder Deposition System Through Process Characterization," SAMPE '95 Proc. p1029.

13) Alloy Digest Typical Value (guage length of 5.8 cm), ASM International p ss-114.



* This work was performed at Sandia National Laboratories supported by the U. S. Department of Energy under contract number DE-AC04-94AL85000.